J Mater Sci (2007) 42:5941–5948
DOI 10.1007/s10853-007-1716-5

Shear stress measurement in nickel and nickel–60 wt% cobalt during one-dimensional shock loading

J. C. F. Millett · Y. J. E. Meziere · N. K. Bourne

Received: 25 April 2006 / Accepted: 5 December 2006 / Published online: 11 April 2007

Abstract The shear strength of pure nickel (Ni), and its alloy, Ni–60Co (by wt%), has been determined during one-dimensional shock loading in the impact stress range 0–10 GPa. The influence of the reduced stacking fault energy (SFE) for the Ni–60Co has been investigated. The shear strength (τ) and the lateral stress (σ_y) both increase with the impact stress for each material. The shear stress has been found to be higher in the nickel than in the alloy. The progressive decrease of the lateral stress behind the shock front indicates an increase of the shear strength. A more complex mechanism of deformation has been found for the alloy since twin formation has been observed in the microstructure, while none has been seen in nickel. It is thought that mechanical twinning plays a predominant role in the deformation mechanism of the alloy resulting in the reduction of the material strength.

Introduction

The requirement to accurately model high velocity impact events is becoming increasingly important, for example from the military in armour design and defeat, aerospace (bird strike and foreign object damage) and satellite protection from orbital debris. Unfortunately, such events involve a projectile of arbitrary shape, size, material, velocity and impact angle impinging upon a target of equally complex geometry (for example the glacis plate on a tank or aerofoil on an aircraft). The conditions under the impact site will be equally complex, with all states of stress and strain (compression, tension and shear) present. This renders meaningful analysis of the event extremely difficult or even impossible, with only qualitative judgments possible. A simpler approach is to determine materials properties from simple testing geometries where the loading conditions are precisely known, and then use these as input data into models that can then be compared to more realistic impact events. At low (quasi-static) strain-rates, these include tensile or compression tests under one-dimensional stress or plane strain fracture toughness. At intermediate strain-rates (10^2 to 10^4 s^{-1}), devices such as the compressional Hopkinson bar again load samples under one-dimensional stress. As strain-rate is increased still further, inertial factors make one-dimensional stress impossible, and hence different techniques are employed. One such is that of plate impact. In this situation, an accurately machined flyer plate of known response is accelerated either explosively or using a gun (powder or gas driven), onto an equally accurate plate of the material of interest, which is instrumented such that useful information may be extracted. The conditions of impact are such that a planar shock wave is driven into the target, which due to inertial confinement results in conditions of one-dimensional strain behind it, thus,

$$\varepsilon_x \neq \varepsilon_y = \varepsilon_z = 0 \quad \text{and} \quad \sigma_x \neq \sigma_y = \sigma_z \neq 0, \tag{1}$$

J. C. F. Millett (✉) · Y. J. E. Meziere
Defence Academy of UK, Cranfield University, Shrivenham, Swindon SN6 8LA, UK
e-mail: Jeremy.Millett@awe.co.uk

Present Address:
J. C. F. Millett
AWE, Aldermaston, Reading RG7 4PR, UK

N. K. Bourne
University of Manchester, Manchester M60 1QD, UK

where ε and σ are strain and stress respectively and the subscript x is in the impact axis, with y and z orthogonal to it. A more complete description of shock loading can be found in the review article of Davison and Graham [1].

Alloying allows the materials scientist to manipulate the properties of a material, which can then be optimised for the required application. Whilst this has been done extensively for low strain-rate applications, much less work has been done under high-strain-rate conditions. For this reason, we have chosen to investigate a nickel–60 wt% cobalt solid solution. Although the unit cell of each element is different (face-centred cubic, fcc for nickel and hexagonal close packed, hcp for cobalt), it can be seen from the phase diagram [2] presented in Fig. 1 that this alloy exists as a simple fcc solid solution alloy.

Moreover, from an atomic perspective, nickel and cobalt are very closely matched; they are adjacent in the periodic table (atomic numbers 28 and 27 for nickel and cobalt respectively); atomic weights (nickel = 58.69 and cobalt = 58.93) and atomic radii (135 pm for both atoms) are also similar. It would thus be expected that the addition of cobalt to nickel would have a minimal effect upon the properties of the resultant alloy. However, one parameter that does undergo a significant change is the stacking fault energy (SFE-γ). Gallagher [3], in collating the results of a number of authors showed that the SFE in pure nickel (ca. 200 ergs cm^{-2}) reduced significantly with the addition of cobalt, to between 20 and 80 ergs cm^{-2} at a cobalt concentration of 60 wt%. Therefore in examining this alloy system, we can change one physical characteristic without having additional factors such as atomic mismatch etc having an influence. In a previous investigation [4], we demonstrated that the shock induced equation of state of nickel, the Hugoniot, was little influenced by cobalt additions, either in terms of shock velocity (U_s)—particle velocity (u_p—the velocity of material flow behind the shock front) or stress—particle velocity. Both alloys showed a linear relationship between shock velocity and particle velocity of the form,

$$U_S = c_0 + Su_p, \tag{2}$$

where c_0 and S are the shock parameters. We summarise these results in Table 1, including those tabulated in Marsh [5] and the equivalent parameters for pure cobalt.

Whilst data in the open literature on nickel–cobalt alloys is somewhat scarce (see for example the work of Trunin et al. [6]), work on the shock response of pure nickel is more extensive. Rose et al. [7] studied the effect of prior variations of cold rolling on shock loaded nickel. Their results indicated that the mechanical hardness of the shocked specimens reached a near constant level regardless of previous levels of work. They went on to suggest that stacking faults and twins did not make a significant contribution to the shock hardening process. In contrast, the results of Kressel and Brown [8] showed that for equivalent plastic strains, the dislocation and point defect concentration in shocked nickel was approximately eight times that of cold rolled nickel at 0°C, with presumably a corresponding increase in hardness. Grace [9] also showed that shocked nickel (and copper) under went significant hardening when compared to the undeformed material. Murr and Kuhlmann-Wilsdorf [10] investigated the shocked microstructure of nickel as a function of shock stress amplitude and pulse duration. They showed that deformation occurred via dislocation generation and motion, with the dislocations arranging themselves into cells. At a constant shock stress of 25 GPa, dislocation density and cell size was observed to be near constant. However, they also observed that at a duration of 0.5 μs, the cell structure was not full developed, leading them to suggest that the required time for cell formation was of the order of 1 μs. Cell size was also observed to be inversely proportional to the peak pressure. Greulich and Murr [11] took this work further, showing that initial grain size or orientation had little effect upon the final shocked microstructure. They also observed that twinning became significant at amplitudes above 35 GPa, forming preferentially in grains orientated with [001] parallel to the shock axis. Twin formation also increased with amplitude and grain size. They were also able to obtain empirical relationships between residual strengthening and prior grain sizes and

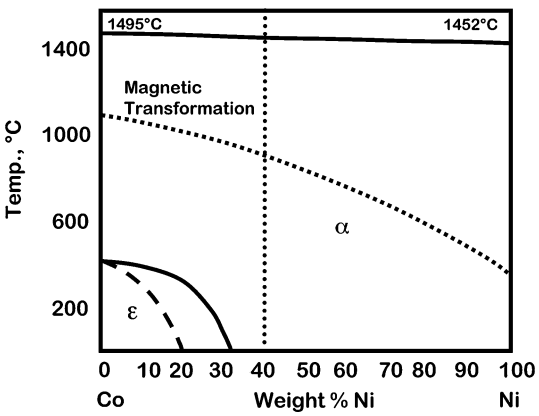

Fig. 1 Phase diagram of the alloy nickel–cobalt [2]

Table 1 Shock parameters

	Ni [4]	Ni–60Co [4]	Ni (Marsh) [5]	Co (Marsh) [5]
c_0 (mm μs^{-1})	4.58	4.65	4.59	4.77
S	1.39	1.41	1.44	1.28
ρ_0 (g cm^{-3})	8.90	8.78	8.88	8.82

shock generated microstructural features. Below 35 GPa (the twinning threshold), the residual strength was seen to have a Hall–Petch type relationship with grain size, with dislocation cell size varying inversely between 0.5 and 1. When twinning occurred, the inter twin spacing was observed to effect residual strength again with a Hall–Petch type effect. Meyers et al. [12] investigated the effects of temperature, shocking nickel at 77 and 300 K. At the lower temperature, the cell structure was less well developed. Contrary to previous workers their results also indicated that at higher pulse durations, the cell size increased. However, they did point out that this was most likely due to a deviation away from one-dimensional strain conditions due to inadequate momentum trapping. Kazmi and Murr [13] repeatedly shocked nickel at 15 GPa and 30 GPa, with each loading cycle lasting 2 μs. Dislocation cell walls were observed to increase in dislocation density at both stress amplitudes, with twinning occurring at 30 GPa. However, twins did not form at 30 GPa for a single load cycle, even at extended pulsed durations, hence showing that repeated load cycles were necessary. Finally, Follansbee and Gray [14] shocked and recovered pure nickel using full lateral momentum trapping techniques [15] on two grain sizes (40 and 225 μm) and two single crystal orientations (<111> and <100>). The recovered microstructures showed dislocation cells, in agreement with previous workers [10], with little difference according to grain size or orientation, although the cells were a little smaller in the single crystals. All samples showed enhanced hardening due to shock loading when compared to the same equivalent strain at quasi-static strain-rates.

Murr and Huang [16] compared the shock response of two simple nickel alloys (Ni–20% Cr and Ni–16% Cr–7% Fe) to that of pure nickel. Both alloys were shown to have a greater preponderance to twin, presumably due to a reduction in SFE. Rohatgi et al. [17–20], in a series of papers examined the role of stacking fault energy on the deformation of a series of copper–aluminium alloys, ranging from pure copper (ca. 78 ergs cm^{-2}) to copper–6 wt% aluminium (ca. 6 ergs cm^{-2}). At quasi-static (ca. 10^{-4} s^{-1}) and intermediate (ca. 1000 s^{-1}) strain-rates [18], they showed an increased preponderance to twin as SFE was reduced. Twinning was also shown to have a significant strengthening effect, in addition to the role of solution strengthening from the aluminium atoms themselves. Under shock loading conditions of 10 and 35 GPa [19], as previously, twinning propensity was seen to increase as aluminium content increased and thus SFE decreased, but due to the extreme strain-rates (ca. 10^6 s^{-1}), all but pure copper and copper–0.2 wt% aluminium shocked to 10 GPa twinned. The authors also recovered samples one-dimensionally for subsequent mechanical testing. They showed that when re-strained, taking into account the equivalent plastic strain applied by the shock, that enhanced hardening *decreased* and that work hardening in the post shocked samples *increased* with decreasing SFE. In high SFE alloys (e.g. pure copper) it was suggested that deformation by rapid dislocation generation during the shock reduced the ability to generate dislocations when reloaded. In contrast, in the low SFE materials, dislocation generation was reduced by the tendency to accommodate the imposed shock strain via twinning, but when re-strained at lower strain-rates, deformation could now be accomplished by dislocation generation. Subsequent analysis of shocked samples by differential scanning calorimetry (DSC) [17] confirmed this, showing that the calculated dislocation density initially increased as SFE decreased (presumably due to an increase in work hardening) but either levelled out or decreased as SFE decreased further. Schneider et al. [21, 22], in laser shocking copper 2 and 6 wt% aluminium alloys also showed an increased likelihood of twining as SFE reduced.

The shock induced mechanical properties of nickel and it's alloys (the Hugoniot Elastic Limit, HEL, yield stress under one-dimensional strain conditions and dynamic tensile–spall strength) appear less well documented. Dandekar and Martin [23] examined the shock response of Mar-M200, a nickel based superalloy, showing that the material underwent substantial precursor decay. Zaretsky et al. [24] investigated two superalloys under shock as a function of temperature. They showed that the strength of these materials gradually decreased with temperature until an abrupt increase between 550 and 600 °C. This they attributed to variations in the heat capacity associated with the equilibration of short-range order in the fcc matrix of these materials. Our own work on pure nickel and nickel 60 wt% cobalt [4], on the variation of spall strength with pulse duration has shown that there is little variation in the case of nickel, whilst there is a pronounced increase with pulse duration in the case of the alloy. Microstructural examination of recovered specimens revealed that the alloy was heavily twinned, and hence it is clear that alloying (in this case a reduction in SFE) has a strong effect upon the shock response of even a simple alloy system. We investigate this further by examining the shear strength (τ) and its variation with time and shock amplitude in these two materials.

Experimental

All shots were performed on 1 50 mm bore, 5 m long single stage gas gun [25]. 8 mm thick plates of nickel and nickel–60 wt% cobalt (flat and parallel to ± 5 μm) were sectioned in half and manganin stress gauges (MicroMeasurements type J2M-SS-580SF-025) were introduced

4 mm from the impact surface. 50 μm mylar on either side of the gauge was used as electrical insulation from the specimens. The target assemblies were reassembled using a low viscosity epoxy adhesive, and held in a special jig for a minimum of 12 h. After removal, the impact faces were relapped to ensure planarity. In this configuration, the gauge is sensitive to the lateral component of stress (σ_y), which in combination with the impact stress (σ_x) can be used to determine the shear strength,

$$2\tau = \sigma_x - \sigma_y. \tag{3}$$

This parameter is particularly useful as it is a good indicator of a materials ballistic performance (resistance to impact damage and penetration) [26]. Voltage data from the gauges were converted to lateral stress using the methods of Rosenberg and Partom [27] with a modified analysis that does not require prior knowledge of the impact conditions [28]. Finally, we also took into account that at low stresses, the geometry of the gauge can have a significant effect upon the results [29]. Longitudinal stresses in the range 1.8–10.2 GPa were generated by the impact of 5 mm flyers of either Dural (aluminium alloy 6082-T6) or copper at velocities of 200 to 500 m s^{-1}. A schematic diagram of the target assembly and gauge placement therein can be seen in Fig. 2.

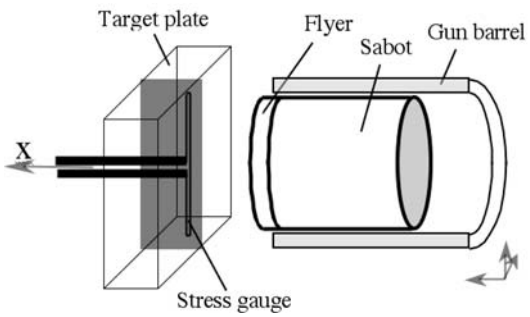

Fig. 2 Specimen configuration and gauge placement

The acoustic properties were measured using 5 MHz quartz transducers with a Panametrics 5072PR pulse receiver.

Material data

Both alloys were supplied (by Special Metals (Wiggins) of Hereford, UK) as forged bar stock. The original ingots were manufactured by casting into a tapered iron mould and then air-cooled. Further processing was via a hammer forging route at 1080 °C. The chemistry and grain size of the as-received materials is presented in Table 2, and the as-received microstructures in Fig. 3.

It can be seen that despite identical forging conditions, the grain size in the alloy is significantly smaller in the alloy than the pure nickel. This can be explained through the effect of stacking fault energy (γ) on the spacing of partial dislocations (d),

$$d = \frac{\mu a^2}{24\pi\gamma} \tag{4}$$

where μ is the shear modulus and a is the lattice spacing. It can be seen that a low SFE (as in nickel 60 cobalt) will result in a high partial spacing. As partial dislocations move in pairs, their spacing will have an effect on their mobility, with a higher spacing enhancing the chances of dislocation tangling and a reduction in the ability to cross-slip. At high temperatures and low strain-rates (as experienced in the forging process), this will result in a greater degree of dislocation generation to accommodate the deformation, and thus a much greater likelihood of dynamic recrystallisation, which will result in a much finer grain size, as observed in Fig. 3. The acoustic properties are presented in Table 3.

The Hugoniots of the two materials were determined in a previous study [4]. The shock parameters, c_0 and S, according to the standard linear relation (Eq. 4), are given

Table 2 Materials composition in weight%

Nickel: Grain size—ca. 200 μm							
C	Si	Mn	P	S	Al	Co	Cr
<0.0005	0.002	<0.001	<0.001	<0.001	<0.001	0.021	<0.001
Cu	Fe	Mg	Ni	Ti	Pb ppm	Zn ppm	O
0.021	0.008	<0.001	Bal.	<0.001	<5	<10	0.0058
Ni–60Co: Grain size—ca. 100 μm							
C	Si	Mn	P	S	Al	Co	Cr
0.004	0.002	<0.001	<0.005	<0.001	<0.001	Bal	0.001
Cu	Fe	Mo	Nb	Ni	Ta	Ti	V
0.003	0.006	<0.001	<0.001	41.9	0.003	<0.001	<0.001

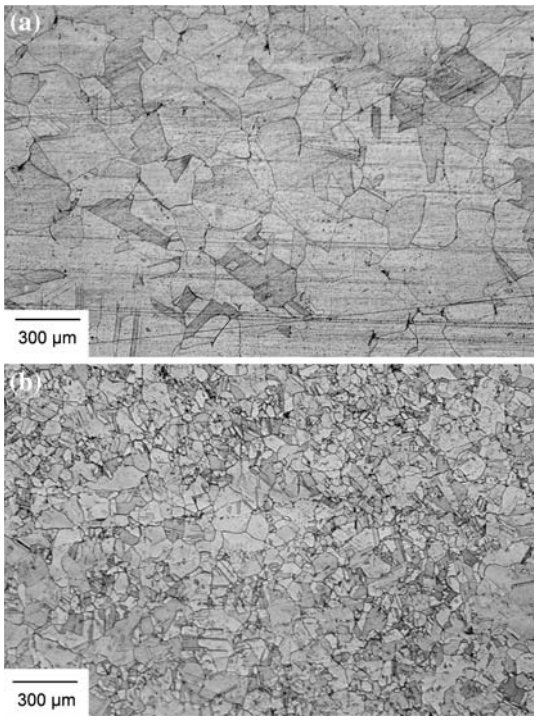

Fig. 3 ''As received'' microstructure: (**a**) nickel (**b**) Ni–60Co

Table 3 Properties of nickel and nickel-60 cobalt

	c_L(mm μs^{-1})	c_S (mm μs^{-1})	ρ_0 (g cm^{-3})	v
Ni	5.83 ± 0.01	3.03 ± 0.01	8.90	0.32
Ni–60Co	5.80 ± 0.01	3.04 ± 0.01	8.78	0.31

c_L, Longitudinal sound speed; c_S, Shear sound speed; ρ_0, ambient density; v, Poisson's ratio

in Table 1, while the Hugoniot (plotted in the ''σ_x–u_p''-space) is shown in Fig. 4. The curve fits are the calculated hydrodynamic pressure, P_{HD},

$$P_{HD} = \rho_0 U_S u_p, \tag{5}$$

where U_S is determined through Eq. 2, using the appropriate values of c_0 and S. The Hugoniots were found to be very similar and a good agreement was noted with the literature data. It was concluded that the reduced SFE of the alloy does not seem to have an effect on the shock induced equation of state [4].

Results

In Fig. 5 we present representative lateral stress gauge traces for both materials. The values in parenthesis are the impact (longitudinal) stress levels for each trace, and the arrows indicate the lateral stress levels used in subsequent calculations.

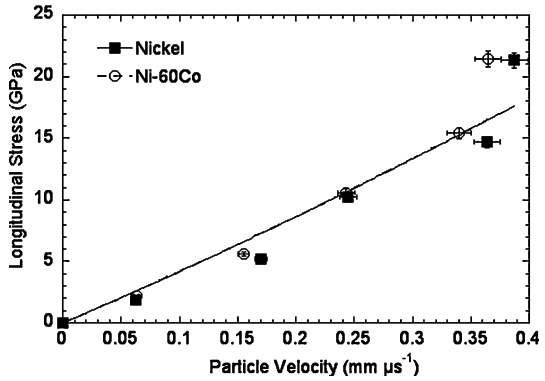

Fig. 4 Shock Hugoniot in the longitudinal stress (σ_x)—particle velocity (u_p) space [4]. The curve fits are according to Eq. 5, using appropriate values of c_0 and S (Table 1)

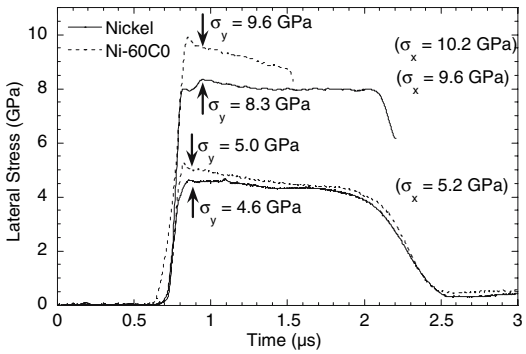

Fig. 5 Typical lateral stress traces for various impact conditions

The slight overshoot in lateral stress is a gauge artifact caused by the fast rising nature of the shock pulse being greater than the response time of the gauge [4]. Observe that in all four traces, that the lateral stress decreases behind the shock front before release waves enter the gauge location. From Eq. 3, this would indicate that the shear strength itself increases slightly behind the shock front.

The lateral stresses measured in Fig. 5 have been used, in combination with the known impact stresses, through Eq. 3 to determine the shear strength of both materials, and its variation with impact stress. The results are plotted in Fig. 6. The fitted curves are simple second order polynomials to indicate trends.

In both cases, shear strength increases with impact stress. However, we note with interest that the pure nickel has higher shear strength under all impact conditions investigated compared to the nickel–cobalt alloy.

In Fig. 5, we noted that the lateral stress decreased (and thus the shear strength increased) behind the shock front in both materials. In Fig. 7, we investigate this further, where we present the rate of change of lateral stress with time ($\Delta\sigma_y/\Delta t$) against impact stress.

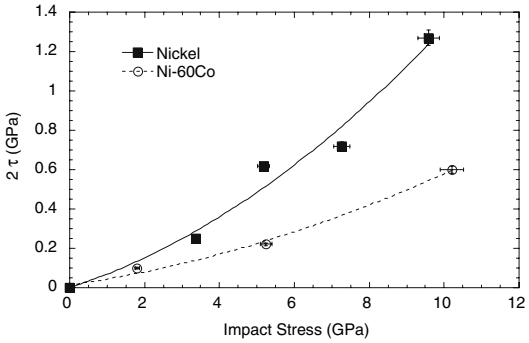

Fig. 6 Shear strength as a function of impact stress. The lateral stress measurement had been made immediately after the impact. The curve fits are simple second order polynomials to indicate trends

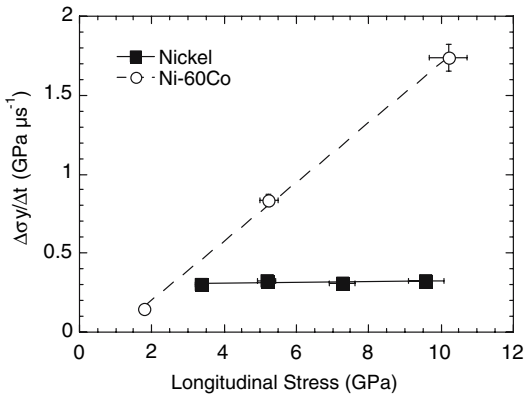

Fig. 7 Decrease of the lateral stress signal as a function of the impact stress. Simple linear regression lines have been fitted to the data to indicate trends

In the case of pure nickel, this appears to be near constant with increasing impact stress, whilst the alloy shows a marked increase. This may well reflect a difference in deformation mechanism (for example it is known that a reduction in SFE can favour twinning over dislocation generation and motion), and it is possible that this result is a reflection of that.

In Fig. 8, we show shocked microstructures of both alloys, to a stress level of ca. 6 GPa. It should be noted that neither of these microstructures was obtained using the full one-dimensional recovery techniques as developed by Gray [15], thus they will have experienced a three dimensional strain state as lateral releases travelled through the specimens. Nevertheless, qualitative differences between the two materials can still yield useful information.

It is clear that in the case of the pure nickel, the shocked microstructure looks little different from the as-received, indicating that the deformation features cannot be resolved optically. In contrast, in the case of the nickel–cobalt alloy, many of the grains show fine linear features across them, indicating the presence of deformation twins.

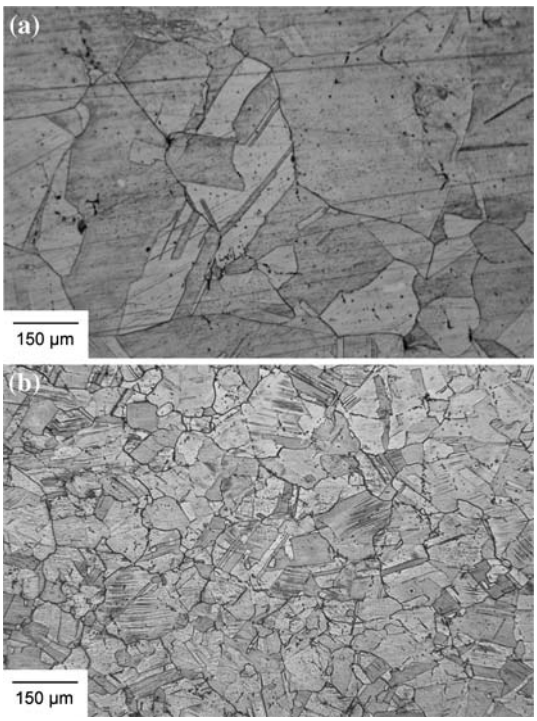

Fig. 8 ''Recovery'' specimens: (**a**) nickel (**b**) Ni–60Co

Discussion

The purpose of this article is to investigate the role of stacking fault energy on the shock response of two otherwise similar materials, in this case pure nickel (high SFE) and nickel 60 cobalt (low SFE). We have chosen to do so by examining how lateral stress changes both with time behind the shock front, and with impact stress, imposed by the conditions of flyer plate material and impact velocity. Previous work has shown that lateral stress response behind the shock front has a strong correlation with deformation mechanism. For example in brittle materials such as glasses [31, 32] or ceramics [33, 34], a two step lateral stress trace is indicative of front travelling behind the main shock, behind which shear strength drops, which has been interpreted as a failure front. In metals, the behaviour is somewhat more subtle but still significant. In body centred cubic metals such as tantalum [35], the lateral stress has been shown to show a gradual increase in lateral stress, indicating a corresponding decrease in shear strength. This was explained in terms of dislocation generation and motion. In the case of tantalum, the high Peierls (lattice friction) stress restricts the generation of new dislocations in the early stages of deformation. If the material in it's pre-shocked state is annealed, then the dislocation density (ρ) will be low and thus the high imposed strain-rate ($\dot{\gamma}$) from the shock will result in a high dislocation velocity (v) through the Orowan relation,

$$\dot{\gamma} = \rho b v \tag{6}$$

where b is the Burger's vector. As the dislocation velocity is so high, the required driving stress will also be high. However, at later stages of deformation, dislocation density increases, so if the strain-rate remains constant, the dislocation velocity, and hence the driving stress will drop, resulting in the observed increase in lateral stress. A decrease in lateral stress (and thus an increase in shear strength) has also be observed in a number of materials including γ-titanium aluminides [36] and very recently, the shape memory alloy NiTi [37] and the ordered nickel–aluminium alloy, Ni_3Al [38]. It was suggested that this was due to an extremely rapid build up of dislocation density and/or twinning. However, all these materials possess ordered variants of simpler unit cells and in the case NiTi, a stress induced martensitic phase transformation as well, thus deformation will be somewhat more complex than in materials with simpler unit cells such as the nickel and the nickel cobalt alloy. From Fig. 5, it can clearly be seen that there is a decrease in lateral stress for these two materials. This is a strong indication that the microstructure evolves for the duration of the shock pulse (at least in this series of experiments). We note with interest that in the recovery experiments performed by Murr and Kuhlmann-Wilsdorf [10] on pure nickel, that at a stress of 25 GPa, the shock generated dislocation cell structure was not fully developed by 0.5 μs, and thus the lateral stress behind the shock front will not reach a constant value. It also suggests that at the lower stresses in this investigation (10 GPa and below), the time required for the dislocation cell structure to fully develop in our own pure nickel may be greater, and thus a constant lateral stress level may never be reached for the applied pulse duration in this series of experiments. The situation with the nickel 60 cobalt is somewhat more complex due to it's much lower stacking fault energy. We have shown in Fig. 8 that it has a greater propensity to twin than it's pure counterpart. We have also shown that it has a significantly lower shear strength than pure nickel (Fig. 6) but in contrast the rate of strengthening behind the shock front is much greater (Fig. 7). From the work of Rohatgi and his colleagues [17–20], it has been shown that as SFE reduces in copper–aluminium alloys, the proportion of plastic deformation from the shock front accommodated by twinning increases, and thus that accommodated by dislocation generation and motion decreases. In addition, the post shock strength of the material also decreases with increasing SFE, and was explained in terms of the reduced dislocation contribution to deformation during the shock process. Therefore the reduced shear strength behind the shock in nickel–60 cobalt in comparison with pure nickel is likely due to the same effects as seen in the copper–aluminium system. Finally, the difference in hardening rate (i.e. $\Delta\sigma_y/\Delta t$) between nickel and nickel 60 cobalt (where is greater in the alloy) has also to be explained. Again, a clue lies in the work of Rohatgi et al. [17–20]. As well as showing that as SFE reduces, deformation during shock loading is increasingly accommodated by twinning, they also show that twins act as effective barriers to dislocation motion. Therefore, it is hypothesised that although the overall dislocation in the alloy is lower, the rate of change with time is greater due to the presence of twins restricting their motion, thus resulting in the greater degree of change in lateral stress behind the shock front.

Conclusions

The shock response of pure nickel and a simple alloy (nickel 60 wt% cobalt) has been monitored using manganin stress gauges mounted such that they were sensitive to the lateral component of stress. In both materials, it was observed that the lateral stress decreased behind the shock front, indicating that they underwent strengthening for the duration of the shock pulse. However, when the lateral stresses were used to determine the shear strengths as a function of impact stress, it was noted that clear differences occurred, with the pure metal being significantly stronger. It is known that cobalt additions to nickel greatly reduce the stacking fault energy (SFE), which in turn results in a shift in plastic deformation mechanism from dislocation generation and motion to form cells to one more dominated by twinning, a was observed from recovered shocked microstructures. We propose that in the alloy, as a large part of the plastic deformation generated by passage of the shock front is accommodated by twinning, the reduced contribution from dislocations results in a reduction of strength behind the shock front. This is in agreement with the work of others who have shown that the post shock hardness of copper–aluminium alloys reduces as increasing aluminium content reduces the stacking fault energy. We have also observed that the rate of hardening behind the shock front is greater in the alloy than in the pure metal. We have proposed that the barriers to dislocation motion provided by twin formation increases the rate of dislocation formation, which manifests as the increase in rate of change of lateral stress behind the shock front.

Acknowledgements The authors would like to thank Matt Eatwell, Ivan Knapp and Adrian Mustey for valuable technical support. Andrew Wallwork and Andrew Workman of AWE (Atomic Weapon Establishment) are thanked for their interest and encouragement. This research was funded by the Engineering and Physical Sciences Research Council (Grant no. GR/S07476/01).

References

1. Davison LW, Graham RA (1979) Phys Rept 55:255
2. Hansen M (1958) Constitution of binary alloys. Mc Graw-Hill, London
3. Gallagher PCJ (1970) Met Trans 1:2429
4. Meziere Y, Millett JCF, Bourne NK (2007) Int J Impact Eng 34:360
5. Marsh SP (1980) Shock Hugoniot data. University of California Press, Los Angeles
6. Trunin RF, Belakiova MY, Zhernokletov MV, Sutulov YN, Izv. Akad. Nauk. SSSR, Fiz Zemli (1991) Bull Acad Sci USSR, Phys. of the solid Earth, 99–109
7. Rose MF, Berger TL, Inman MC (1967) Trans Met Soc AIME 239:1998
8. Kressel H, Brown N (1967) J Appl Phys 38:1618
9. Grace FI (1969) J Appl Phys 40:2649
10. Murr LE, Kuhlmann-Wilsdorf D (1978) Acta Metall 26:847
11. Greulich F, Murr LE (1979) Mater Sci Eng 39:81
12. Meyers MA, Kestenbach HJ, Soares CAO (1980) Mater Sci Eng 45:143
13. Kazmi B, Murr LE (1981) In: Meyers MA, Murr LE (eds) Shock waves and high-strain-rate phenomena in metals. Plenum, New York, pp 733–752
14. Follansbee PS, Gray GT III (1991) Int J Plast 7:651–660
15. Gray GT III (1992) In: Meyers MA, Murr LE, Standhammer KP (eds) Shock-wave and high strain rate phenomena in materials. Marcel Deker, New York, pp 899–911
16. Murr LE, Huang J-Y (1975) Mater Sci Eng 19:115
17. Rohatgi A, Vecchio KS (2002) Mater Sci Eng A328:256
18. Rohatgi A, Vecchio KS, Gray GT III (2001) Met Mater Trans A 32A:135–145
19. Rohatgi A, Vecchio KS, Gray GT III (2001) Acta Mater 49:427
20. Rohatgi A, Vecchio KS, Gray GT III (2001) In: Staundhammer K, Murr L, Meyers Elsevier M (eds) Fundamental issue and applications of the shock-wave and high-rate phenomena. Amsterdam, pp 25–32
21. Schneider MS, Kad B, Kalantar DH, Remington BA, Kenik E, Jarmakani H, Meyers MA (2005) Int J Impact Eng 32:473
22. Schneider MS, Kad BK, Gregori F, Kalantar DH, Reminton BA, Meyers MA (2004) Mater Sci Forum 465–466:27
23. Dandekar DP, Martin AG (1980) In: Meyers MA, Murr LE (eds) Shock waves and high-strain-rate phenomena in metals, Plenum, New York, pp 573–587
24. Zaretsky EB, Kanel GI, Razorenov SV, Baumung K (2005) Int J Impact Eng 31:41
25. Bourne NK (2003) Meas Sci Technol 14:273
26. Meyer LW, Behler FJ, Frank K, Magness LS (1990) In: Antonio S (ed) 12th Int. Symp. Ballistics, Texas, pp 419–428
27. Rosenberg Z, Partom YJ (1985) J Phys D Appl Phys 58:3072
28. Millett JCF, Bourne NK, Rosenberg Z (1996) J Phys D 29:2466
29. Rosenberg Z, Bourne NK, Millett JCF (2006) In: Furnish MD (ed) Shock compression of condensed matter – 2006. AIP Press, Melville, NY, pp 1207–1210
30. Bourne NK, Rosenberg Z (1997) Meas Sci Technol 8:570
31. Brar NS, Bless SJ (1992) High Pressure Res 10:773
32. Kanel GI, Razorenov SV, Savinykh AS, Rajendran A, Chen Z (2005) J Appl Phys 98:113523
33. Bourne N, Millett J, Murray N, Rosenberg Z (1998) J Mech Phys Solids 46:1887
34. Millett JCF, Bourne NK (2001) J Mater Sci 36:3409
35. Gray GT, Bourne NK, Millett JCF (2003) J Appl Phys 94:6430
36. Millett JCF, Bourne NK, Gray GT III, Jones IP (2002) Acta Mater 50:4801
37. Meziere YJE, Millett JCF, Bourne NK (2006) J Appl Phys 100:033513
38. Millett JCF, Meziere YJE, Gray GT III, Cerreta EK, Bourne NK (2006) J Appl Phys 100:063506